ENGINEER - Vol. LIX, No. 01, pp. [47-58], 2026

DOI: https://doi.org/10.4038/engineer.v59i1.7732

CFD Analysis of Transition & Turbulent Flow Through Pipes

N.P.H. Abeyagunawardana, I.U. Atthanayake and T.M.D.N. Tennekoon

Abstract: Accurate prediction of the pipe pressure loss is important for engineering applications. But the Reynolds number does not definitively determine whether the flow is laminar or turbulent. Therefore, relying solely on Reynolds number to select the specific equation can be inaccurate, as the actual flow regime might differ from prediction. In this study, computational fluid dynamics (CFD) simulations were conducted using the ANSYS fluent 2023 R2 with the standard k–ε turbulence model and standard wall functions to analyze fully developed pipe flow across Reynolds numbers from 2,000 to 200,000, with varying wall roughness values. A mesh-independence study verified convergence beyond approximately 0.7×10^6 cells. The investigation systematically varied the inlet velocity and the surface roughness to quantify their effects on pressure loss; this simulated result was compared against theoretical predictions using the Darcy–Weisbach and Colebrook–White equations for transitional and turbulent flow. The findings revealed that CFD consistently predicted below 20% pressure losses in turbulent flow than theoretical models, particularly in the transitional regime where more than 200% difference was observed, highlighting limitations of conventional methods. Pressure loss was found to increase significantly with the inlet velocity, while the surface roughness exhibits comparatively minor influence. These results emphasize the importance of velocity control that minimizes energy loss in piping systems and demonstrate the capability of CFD to provide deep insight into pipe flow.

Keywords: Computational Fluid Dynamics (CFD), K-epsilon, Pipe Flow, Pressure Loss, Surface Roughness, Transition and Turbulent Flow

1. Introduction

Transition and turbulent flow through pipes constitute fundamental phenomena in fluid dynamics, with significant implications for various industries. These aspects encompass the exploration of characteristics, modelling, experimental investigations, computational approaches, and flow control strategies related to transition and turbulent flow in pipe systems. The understanding and accurate prediction of these flow regimes are crucial for optimizing pipe designs, minimizing energy losses, and enhancing system efficiency. Transition and turbulent flow through pipes constitute dynamic and complex phenomena that have undergone extensive study.

Osborne Reynolds published his famous paper entitled ‘‘An experimental investigation of the circumstances which determine whether motion of water shall be direct or sinuous and of the law of resistance in parallel channels’’ [1] could shift the onset of turbulence from Re ≈ 2,000 to 13,000 by reducing disturbances at the pipe inlet. However, subsequent experiments have demonstrated the ability to maintain laminar flows, even at Reynolds numbers as high as 100,000[2]. Thus, solely relying on the Reynolds number may not accurately determine whether the flow is laminar or turbulent.

Theoretical friction loss values are calculated using the Darcy-Weisbach equation (Eq 1) and the friction factor f is calculated using the Colebrook-White equation (Eq 2) for the turbulent regime and Eq 3 for the laminar regime. While Colebrook-White equation is accurate for the turbulent flow regime (Re > 4000), definitively determining the flow regime

__Eng. N.P.H. Abeyagunawardana__, AMIE(SL), B.Sc. Eng (Hons)(OUSL), AEng EC(SL), Lecturer on Contract, The Department of Mechanical Engineering,
The Open University of Sri Lanka,
Email:s18001025@ousl.lk/hashelabeyagunawardana@gmail.com
ORCID ID:https://orcid.org/0009-0005-8905-712X
__Eng. (Dr.) (Mrs.) I.U. Atthanayake,__ AMIE(SL), B.Sc. Eng. (Hons)(Peradeniya), Mphil (UOM), PhD (Warwick), Senior Lecturer, The Department of Mechanical Engineering, The Open University of Sri Lanka,
Email:iuatt@ou.ac.lk
ORCID ID:https://orcid.org/0000-0002-6667-2008
__Eng. (Mrs.) T.M.D.N. Tennekoon,__ CEng, MIE(SL), B.Sc. Eng. (Hons)(Peradeniya), M.Phil(SHU), MIEEE, ECSL, Senior Lecturer, The Department of Mechanical Engineering,
The Open University of Sri Lanka,
Email:tmmed@ou.ac.lk/nimalim@yahoo.com
ORCID ID:https://orcid.org/0000-0002-7210-0874

based solely on the Reynolds number remains a challenge. Due to this uncertainty, selecting the appropriate equation is difficult. For instance, flow can remain laminar even at Reynolds numbers as high as 100,000[2]. Using a CFD approach can mitigate some of the challenges. While Computational Fluid Dynamics (CFD) does not depend on the Reynolds number to solve the governing equations, the selection of an appropriate turbulence or transition model presents a significant challenge. Therefore, this study aims to address those issues and present a better solution.

$$\Delta P = f\,\frac{\rho L U^2}{2D} \quad \text{... (1)}$$

$$\frac{1}{\sqrt{f}} = 1.14 - 2\,log_{10}\left(\frac{e}{D} + \frac{9.35}{Re\sqrt{f}}\right) \quad \text{... (2)}$$

$$f = \frac{64}{Re} \quad \text{... (3)}$$

2. Computational Fluid Dynamics Approach for the Pipe Flow

Computational Fluid Dynamics (CFD) serves as a powerful research tool in various scientific and engineering disciplines. CFD simulations can save time and money compared to traditional experimentation and testing methods, CFD simulations can provide a deeper understanding of the flow behaviour and physical phenomena within a system, allowing engineers and scientists to make informed design decisions [3,4]. Most importantly, the number of schemes and methods on which CFD is based rapidly evolves, increasing the reliability of CFD-produced outcomes. Increasing reliability makes CFD a reliable tool for any design or analytical task. Modern industrial CFD codes are very reliable under accurate boundary conditions, grid size and correct mathematical model.

Turbulence modelling for pipe CFD often uses Reynolds Averaged Navier Stokes (RANS) closures. The standard k- ε model is widely used for industrial flow due to its simplicity and robustness. Standard and enhanced wall treatment or wall functions are applied to high Reynolds flow near the wall [3,4]. Reference [5] found that a standard k-ε model with appropriate wall treatment can accurately predict fully developed turbulent friction factors. Although more advanced models (RANS–LES hybrids, Reynolds-stress models) exist, RANS remains common in pipe flow design. Wall roughness introduces additional pressure loss, reviews of roughness effects [6] show that rough surfaces increase turbulent friction, while velocity scaling remains dominant.

To calculate the friction factor *f* in the Colebrook-White equation, Newton-Raphson iterative numerical method was used; Due to the implicit nature of the equation, friction factor cannot be isolated algebraically. The solution process was initialized using the explicit Haaland approximation as a starting value, and iterations were performed until the residual error dropped below a strict convergence tolerance of $10^{-6.}$ This approach ensures that the theoretical pressure loss values are precise and eliminates reading errors associated with the manual use of the Moody diagram.

However, standard k- ε Model is not formulated to capture the physics of the laminar-to-turbulent transition. While transition sensitive models such as $k\text{-}k_l\text{-}w$ or transition SST are theoretically superior for identifying the onset of turbulence, the standard k- ε model was selected for this study to reflect common industrial CFD practices. It is acknowledged that this model assumes fully turbulent flow and uses standard wall functions, effectively bypassing the laminar sub-layer transition. Furthermore, since the Reynolds number alone is often an unreliable indicator of the exact laminar-to-turbulent transition point, relying on a fully turbulent model avoids the regime prediction. Consequently, it is expected that the model will over-predict skin friction coefficients in the transition regime ($2000 < Re < 4000$) by forcing turbulent viscosity values before they physically occur. Therefore, the results presented herein should be interpreted as a conservative upper bound for pressure loss, serving to quantify the deviation inherent in standard high-Reynolds-number modeling approaches when applied to transitional flow regimes.

3. Mathematical Modelling of the Simulation Setup

To analyze the pressure loss due to surface roughness in turbulent and transition condition, conducting accurate CFD simulation is essential. First it is necessary to define the initial parameters and establish the framework for the data flow and process. As demonstrated in Figure 1, this workflow begins with defining initial conditions, parameters and data requirements for the simulation. For the simulation, a 3D cylindrical pipe with a diameter(D) of 0.05 m and a length(L) of 1 m was selected, resulting in a length-to-diameter ratio (L/D) of 20. It is noted that for turbulent flow, the hydrodynamic entrance length (L_e) required to achieve fully developed flow conditions is estimated by the correlation $L_e/D = 4.4\ Re^{1/6}$.

At the maximum simulated Reynolds number of 200,000 the required entrance length is approximately 33D (1.68 m). Since the modeled domain (20D) is shorter than the entrance length, the fluid remains in the developing flow regime throughout the pipe. In this entrance region, the boundary layer is developing, resulting in higher velocity gradients at the wall and, consequently, higher wall shear stress compared to the fully developed region. This explains the trend observed in the results, where the CFD-predicted pressure losses exceed the theoretical values derived from the Darcy-Weisbach equation which assumes fully developed conditions. This geometry was retained to simulate compact piping sections, such as industrial heat exchangers and valve assemblies, where fully developed flow is often not established.

The standard K-epsilon (k-ε) turbulence model with standard wall function was selected for accurate unsteady state simulation of wall effects and the turbulence conditions. The simulation was executed and validated, with mesh refinements applied where necessary to achieve acceptable y^+ values and realistic results. Finally, the data were analysed to identify patterns and relationships and represent them.

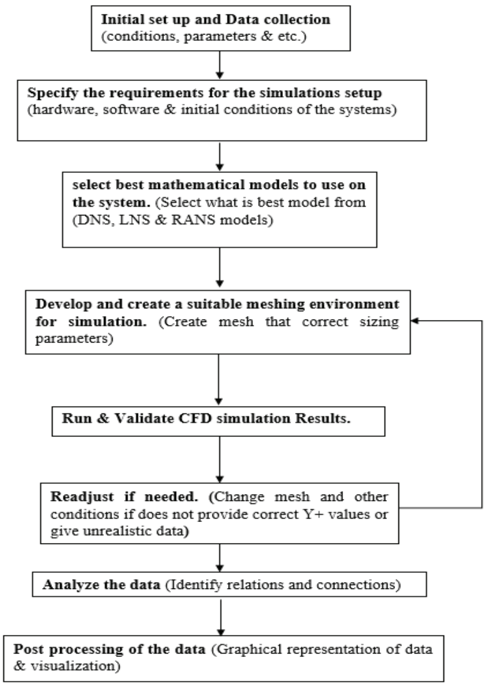

Figure 1- Schematic diagram of the CFD simulation methodology

3.1 Governing Equation for the CFD Simulation

Computational fluid dynamics (CFD) simulations of pipe flow are based on the numerical solutions of the fundamental governing equations for fluid motion which are derived from the principles of conservation of mass, momentum and, when necessary, energy. For an incompressible Newtonian fluid, the flow is described by the continuity (Eq 4) and Navier-stokes (Eq 5) equations.

$$\frac{\partial \rho}{\partial t} + \frac{\partial}{\partial x}\rho u_x + \frac{\partial}{\partial y}\rho u_y + \frac{\partial}{\partial z}\rho u_z = 0 \qquad \text{... (4)}$$

$$\rho\frac{D}{Dt}v = -\nabla p + \rho g + \mu\nabla^2 v \qquad \text{... (5)}$$

In Eq 4, ρ denotes the fluid density, U_x, U_Y, and U_Z, are the velocity components in the X, Y, and Z directions, and t denotes time. The first term represents the local time rate of change of density, while the remaining terms represent the convective transport of mass in each coordinate direction. When considering the momentum equation (Eq 5) V is the velocity vector, P is the static pressure, g is the gravitational acceleration vector and μ is the dynamic viscosity. The term $\rho\frac{D}{Dt}v$ represents the material acceleration, $-\nabla p$ accounts for the pressure gradient force, ρg denotes body forces due to gravity and $\mu\nabla^2 V$ represents the viscous diffusion.

3.2 Reynolds Average Navier – Stokes Equation (RANS Equation)

In turbulent flow, velocity and pressure exhibit random fluctuations over time. Resolving these fluctuations using direct numerical simulations (DNS) are computationally expensive for most engineering applications including internal pipe flow. To overcome these limitations the Reynolds averaged Navier Stokes (RANS) approaches are used. The Reynolds decomposition method is applied to velocity (Eq 6), pressure (Eq 7), and other variables to distinguish between the mean flow and turbulent fluctuations.

$$u_i = \bar{u}_i + u'_i \qquad \text{... (6)}$$

$$p = \bar{p} + p' \qquad \text{... (7)}$$

Here $\bar{u}_i$ and $\bar{p}$ represent the time-averaged (mean) velocity and pressure, while u'_i and p' are fluctuating components. Substituting those decomposed quantities into the Navier Stokes equation (Eq 5) and performing time-averaging yields the RANS momentum equation (Eq 8).

$$\rho\frac{\partial \bar{u}_i}{\partial t}+\rho\bar{u}_j\frac{\partial \bar{u}_i}{\partial x_j}=-\rho\bar{u}_j\frac{\partial \bar{p}}{\partial x_i}+\mu\frac{\partial^2\bar{u}_i}{\partial x_j^2}-\frac{\partial}{\partial x_i}(\rho\overline{u_i'u_j'}) \quad \text{... (8)}$$

The first four terms in the equation correspond to the mean flow physics; unsteady acceleration, convection, pressure gradient, and viscous diffusion. The term represents the Reynolds stress, which arises from the correlation of turbulent viscosity fluctuations. These stresses introduce six additional unknowns into the system of equations, making the RANS formulation unclosed. This is known as the closure problem in turbulence modeling. To close the equations, turbulence models are introduced to express the Reynolds stresses in terms of mean flow quantities. Commonly, the Boussinesq hypothesis is applied, which relates the Reynolds stresses to the mean velocity gradients via an eddy viscosity μ_t (Eq 9).

$$-\rho\overline{u_i'u_j'} = \mu_t\left(\frac{\partial \bar{u}_i}{x_j}+\frac{\partial \bar{u}_j}{x_i}\right)-\frac{2}{3}\rho k\delta_{ij} \quad \text{... (9)}$$

where k = $\frac{1}{2}\overline{u'_\iota u'_\iota}$ is the turbulent kinetic energy and δ_{ij} is the Kronecker delta. The RANS equations, combined with a suitable turbulence model such as the standard k-ε model, allow for the accurate prediction of the mean velocity, pressure, and turbulence fields in pipe flows while keeping computational costs significantly lower than those of DNS or Large Eddy Simulation (LES).

3.3 Standard k- ε Turbulence Model with Standard Wall Function

The standard k–ε model, introduced by Launder and Spalding (1974) [7], is one of the most widely used two-equation turbulence models for engineering applications. It is based on the Boussinesq eddy viscosity hypothesis, which relates the Reynolds stresses in the RANS equations to the mean velocity gradients via the eddy viscosity μ_t, as in Eq 10.

$$\mu_t=\rho C_\mu\frac{k^2}{\varepsilon} \quad \text{... (10)}$$

where k is the turbulent kinetic energy and ε is its dissipation rate. These quantities are obtained from their own transport equations, as shown in Eq 11 and Eq 12.

$$\frac{\partial(\rho k)}{\partial t}+\frac{\partial(\rho k u_j)}{\partial x_j}=\frac{\partial}{\partial x_j}\left[\left(\mu+\frac{\mu_t}{\sigma_k}\right)\frac{\partial k}{\partial x_j}\right]+G_k-\rho\varepsilon \quad \text{... (11)}$$

$$\frac{\partial(\rho\varepsilon)}{\partial t}+\frac{\partial(\rho\varepsilon u_j)}{\partial x_j}=\frac{\partial}{\partial x_j}\left[\left(\mu+\frac{\mu_t}{\sigma_\varepsilon}\right)\frac{\partial \varepsilon}{\partial x_j}\right]+C_{1\varepsilon}\frac{\varepsilon}{k}G_k-C_{2\varepsilon}\rho\frac{\varepsilon^2}{k} \quad \text{... (12)}$$

For the turbulent model, following model constants were used for the simulation of the pipe flow, C1-Epsilon ($C_{1\varepsilon}$) = 1.44, C2-Epsilon($C_{2\varepsilon}$) =1.92, Cmu (C_μ)= 0.09, TKE Prandtl Number (σ_k) =1, and TDR Prandtl Number(σ_ε)=1.3 [5]

3.3.1 Standard Wall Function

In turbulent flows, a very fine mesh is needed to resolve the near-wall area, which is computationally costly. Instead, the standard wall function technique uses semi-empirical relations established from experimental data to bridge the gap between the near-wall viscous sublayer and the completely turbulent outer core.

In this approach, the first near-wall mesh is placed in the log-law region around 30<y^+<300, where the dimensionless velocity profile is approximated by Eq 13. Therefore, the accuracy of the simulated results can be verified.

$$\frac{U^+}{k}=\ln(y^+)+B \quad \text{... (13)}$$

where Eq 14 is the dimensionless mean velocity, Eq 15 is the dimensionless wall distance, Eq 16 is the friction factor. Furthermore, K ≈ 0.41 is the von Karman constant, and $B \approx 5.0$ is an empirical constant.

$$U^+=\frac{U}{u_r} \quad \text{... (14)}$$

$$y^+=\frac{\rho y u_\tau}{\mu} \quad \text{... (15)}$$

$$u_t=\sqrt{\tau_w/\rho} \quad \text{... (16)}$$

The wall shear stress, turbulent kinetic energy, and dissipation rate in the near-wall cells are computed using these empirical relations, allowing accurate prediction of wall friction without fully resolving the viscous sublayer.

4. CFD Simulation Setup

The CFD simulation was conducted using ANSYS 2023 R2 version [8]. A pipe geometry with a length of 1 m and a diameter of 0.05 m was selected for the simulation and ANSYS Design Modeler was used to construct the model of the pipe. Table 1 shows the properties of the selected fluid.

Table 1- Fluid properties for selected system

Property	Units	Value
Density	kg/m³	998.2
Cp (Specific Heat)	J/(kg K)	4182
Viscosity	kg/(m s)	0.001003
Thermal Conductivity	W/(m K)	0.6
Molecular Weight	kg/kmol	18.0152

Table 2 shows the discretization setup, specifying the numerical scheme applied to transform the governing flow equations into a solvable algebraic form over the computational domain. It defines the spatial and temporal approximation methods for variables such as pressure, velocity and turbulence quantities, which directly influence the accuracy, stability and convergence of the simulation results. Table 3 shows the time step setup from the CFD simulation that specifies the physical run time of the simulation.

Table 2- Discretization setup from the CFD simulation

Property	Methode
Pressure velocity coupling	SIMPLE
Gradient	Lest Squares cell based
Pressure	Second order
Momentum	Second order upwind
Turbulent kinetic energy	First order upwind
Turbulent dissipation rate	First order upwind
Transient formulation	First order implicit

Table 3- Time step setup from the CFD simulation

Property	Value
Time step size(s)	0.25
Number of time steps	240
Max iteration per time step	100

4.1 Mesh and the Mesh Independent Study

The purpose of a mesh independence study is to assess the sensitivity of the simulation results to changes in the mesh resolution. Specifically, it aims to determine if the results are converged and become insensitive to further mesh refinement, indicating that the solution is independent of the mesh.

Mesh Independence Test was conducted for the selected pipe geometry using the standard K-epsilon with standard wall function. Element sizing was changed using the number of circumferential divisions along the pipe's circular edge. In total, 22 data points were considered and the below Figure 2 represents the simulation data, plotting the number of mesh elements against the maximum velocity at the pipe outlet.

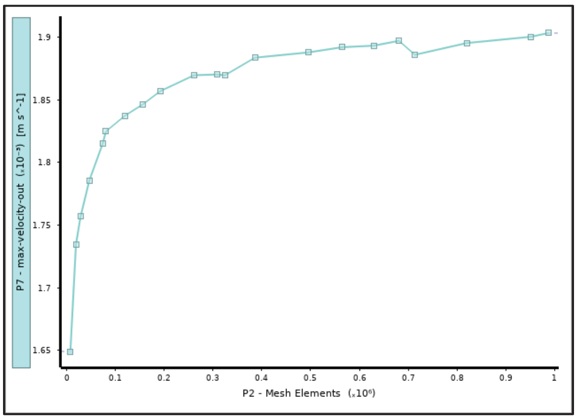

Figure 2 – Number of mesh elements vs max velocity at the outlet

Analysis of Figure 2 demonstrates that after data point 18, the mesh independence is achieved. It is clearly demonstrated in Figure 2, max velocity at outlet values does not change considerably with respect to the mesh elements after 0.7 million, further mesh refinement may not significantly improve the accuracy of the results but will increase computational costs. Because of that optimum number of divisions was 100 for the pipe's circular edge. To achieve an acceptable y^+ value, an inflation layer was constructed near the pipe wall according to the Eq15.

In addition to mesh independence test, it is critical to determine the nature and the distribution of cells in the geometry. Skewness, aspect ratio, element quality and orthogonal quality values were analysed, and all were within the acceptable limits for simulation.

5. Transition & Turbulent Simulation of the Pipe Flow

Figure 3 illustrates the integrated workflow implemented within ANSYS Workbench. The core computational analysis is performed using the Ansys Fluent system (Component A), where the initial physics configurations were established and the parametric input/output variables were defined. To efficiently generate and explore a broader range of data points specifically across the transitional and turbulent regimes a Response Surface Optimization (Component B) module was coupled with the solver. Response Surface Optimization (RSO) method constructs a mathematical metamodel (response surface) based on discrete design points calculated by the CFD solver. By interpolating between these points, the RSO creates a continuous predictive model, enabling the identification of non-linear trends in pressure drop relative to inlet velocity and surface roughness across the entire design space.

Finally, to interpret the trends and quantify the dependencies between variables, a Parametric Correlation (Component C) tool was utilized. This process statistically evaluates the linear and non-linear dependencies between the input parameters (inlet velocity, wall roughness) and the output response (pressure drop). By calculating correlation coefficients (such as Pearson or Spearman rank), this analysis identifies the dominant factors driving energy loss, thereby substantiating the finding that pressure drop is significantly more sensitive to variations in flow velocity than to changes in surface roughness within the studied range.

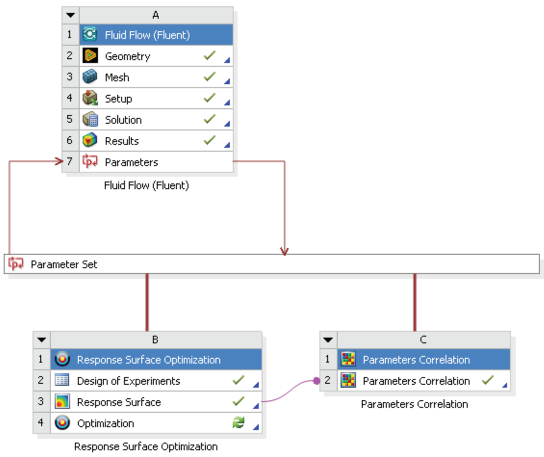

Figure 3 – Project workflow and the schematic diagram

Boundary conditions

Inlet

- Type- velocity inlet.
- Inlet Velocity (Parametrized) - 0.04m/s to 4m/s (Renolds number 2000 to 200,000)
- Reference Frame Absolute
- Velocity magnitude normal to boundary -Z direction
- Turbulence Intensity 5 %
- Hydraulic Diameter 0.05

Outlet

- Type- Pressure outlet.
- Outlet gauge pressure - 0
- Reference Frame- Absolute
- Backflow Direction Specification method- Normal to boundary
- Turbulence Intensity 5 %
- Hydraulic Diameter 0.05

Pipe Wall

- Stationary wall with no slip
- Roughness height (Parametrized) – 9E-07m to 0.001m
- Roughness constant – 0.5

5.1 Contour Plots of the Simulation

For the visual analysis of the flow, pressure and velocity contours were extracted at multiple locations and at different time intervals to capture both spatial and temporal variations. As illustrated in Figure 4 and Figure 5, the results clearly indicate a continuous and measurable pressure drop along the downstream section of the pipe, consistent with theoretical expectations for internal flows. A comparison with Figure 6 and Figure 7 reveals the formation of a distinct boundary layer adjacent to the pipe wall, characterized by a slow-moving fluid region where viscous effects dominate. This phenomenon becomes more pronounced at higher inlet velocities, where turbulence intensifies near the wall. Considering the velocity contours in Figure 8 and Figure 9, the boundary layer formation and its progressive thickening along the pipe length are further confirmed. These plots also demonstrate how changes in inlet velocity and wall surface roughness alter the velocity gradient within the near-wall region, influencing shear stresses and turbulence generation. The combined analysis of these contour plots provides valuable insight into the mechanisms governing pressure drop, flow uniformity, and energy losses in both transitional and turbulent regimes.

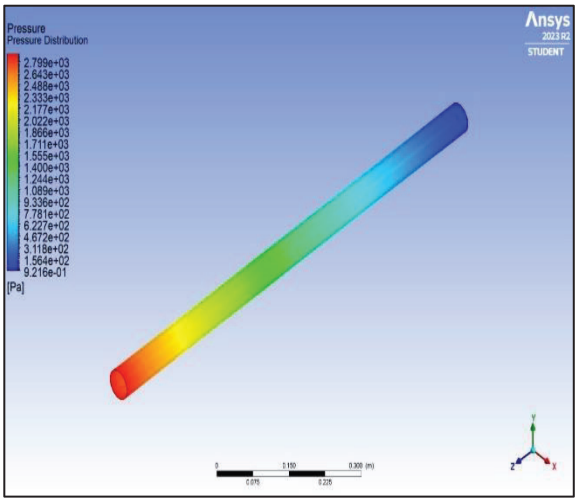

Figure 4-Pressure change in pipe at 4m/s inlet velocity with 9x10^{-7}m surface roughness

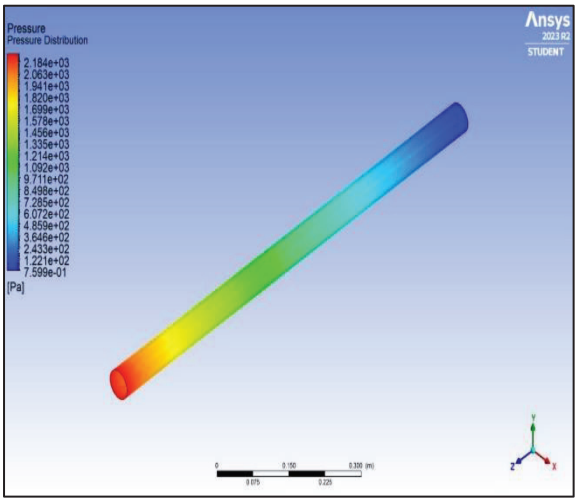

Figure 5- Pressure change in pipe at 2.2 m/s inlet velocity with 5x10^{-4}m surface roughness

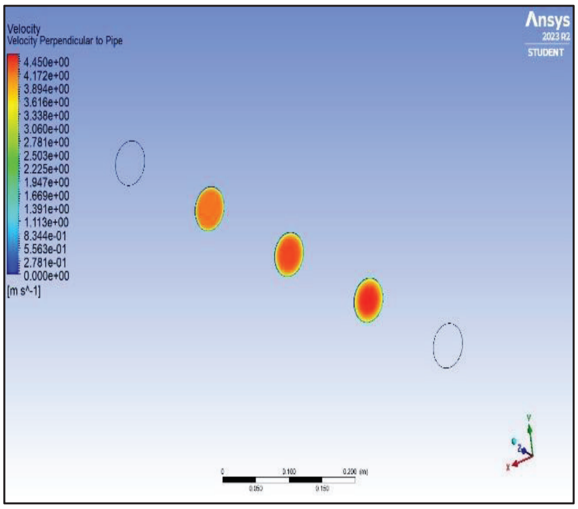

Figure 6- Velocity contours perpendicular to pipe wall at 4m/s velocity with 9x10^{-7} m surface roughness

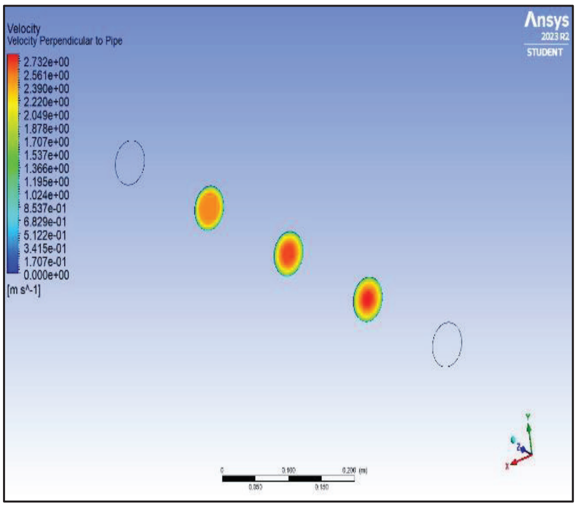

Figure 7- Velocity contours perpendicular to pipe wall at 2.2 m/s velocity with 5x10^{-4}m surface roughness

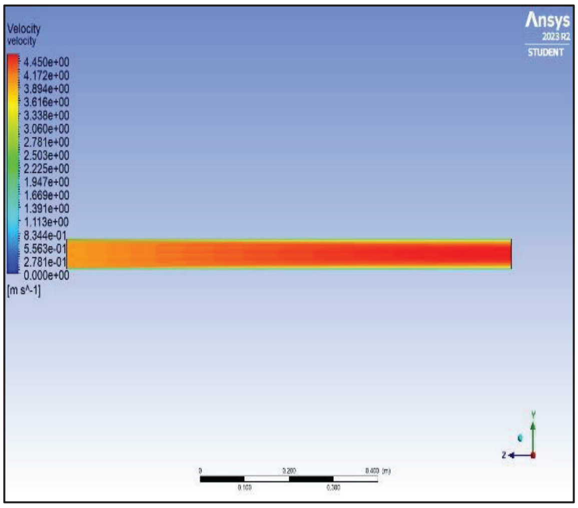

Figure 8- Velocity contour on centre plane at 4m/s Inlet velocity with 9x10^{-7}m surface roughness

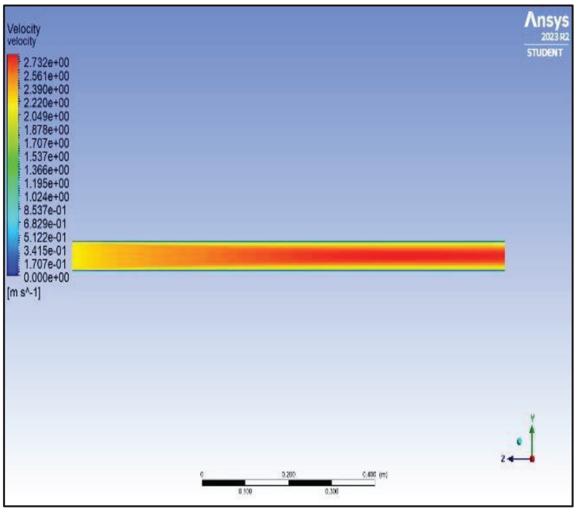

Figure 9- Velocity on centre plane at 2.2m/s Inlet velocity with 5E-04m surface roughness

5.2 Verification of the Turbulent Velocity Profile

Analysis of the turbulent velocity profiles reveals the characteristic shape associated with RANS simulations. Considering the normalized velocity profiles it agrees with the theoretical profile [9]. The theoretical velocity profile was calculated using the Eq 17 [9].

$$\frac{u}{u_{max}} = \left[1 - \left(\frac{r}{R}\right)^{m}\right]^{\frac{1}{n}} \qquad \dots (17)$$

For the equation constants m=1 and n=7 were taken [9] where U_{max} is the stream velocity and U is the actual turbulence velocity.

Figure 10 clearly shows an agreement with the theoretical velocity profile with the CFD simulated velocity data. Also, for other condition similar agreement was achieved; because of this results validation and conformation of the turbulence behaviour of the CFD simulation model can be confirmed.

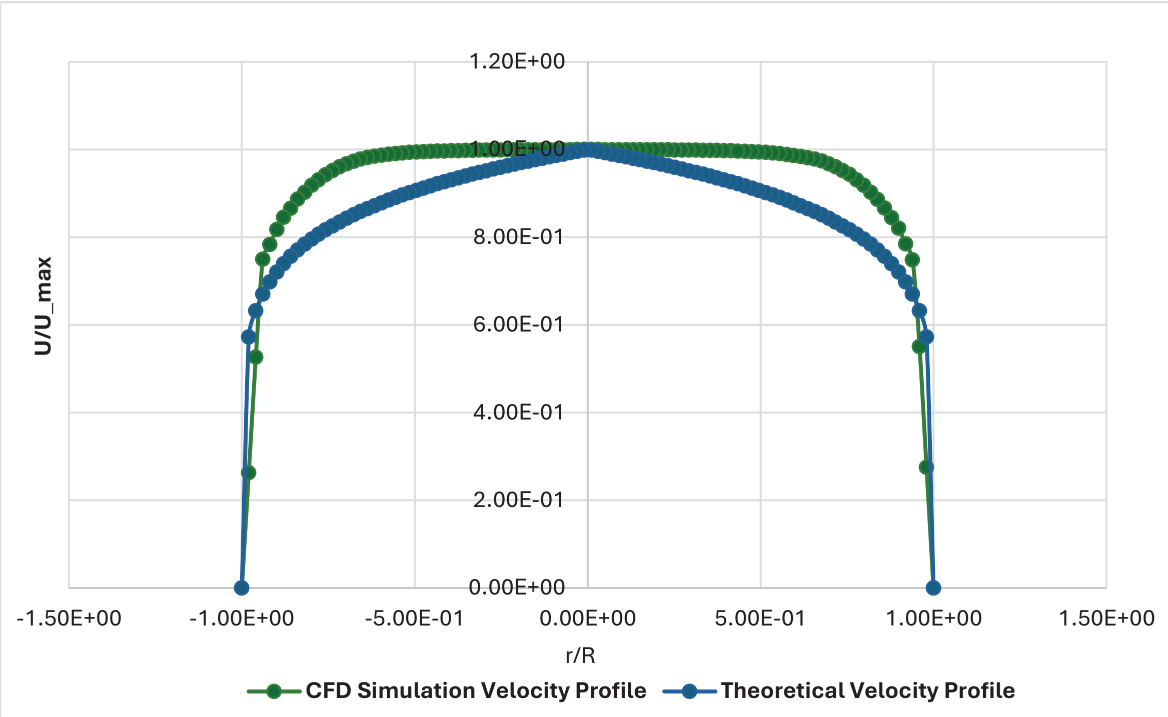

Figure 10- Normalized turbulence flow velocity profiles theoretical and CFD simulated at 4m/s velocity with 9x10^{-07}m surface roughness

5.3 y⁺ Distribution in the Pipe Wall

Regarding the y^+ distribution, all points must remain below 300 and above 30 [10]. Figure 11 depicts the simulation at the maximum velocity condition. Since the y^+ values in this critical case fall within the 30–300 limit, it confirms that all simulation results are within acceptable range.

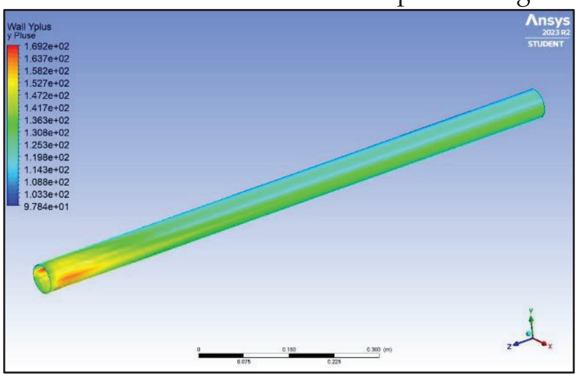

Figure 11 - y^+ distribution of pipe at 4 m/s velocity with 4x10^{-9} m surface roughness

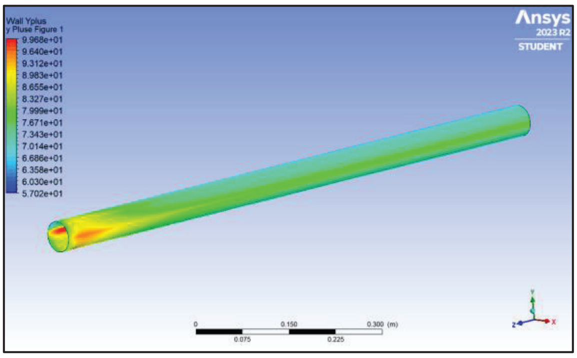

Figure 12- y^+ distribution of pipe at 2.02 m/s with 9E-07 m surface roughness

6. Correlation Between the Surface Roughness, Velocity and Pressure Loss

Considering Figures 13 & 14 they depict the theoretical and CFD simulation pressure loss comparison and its percentage difference.

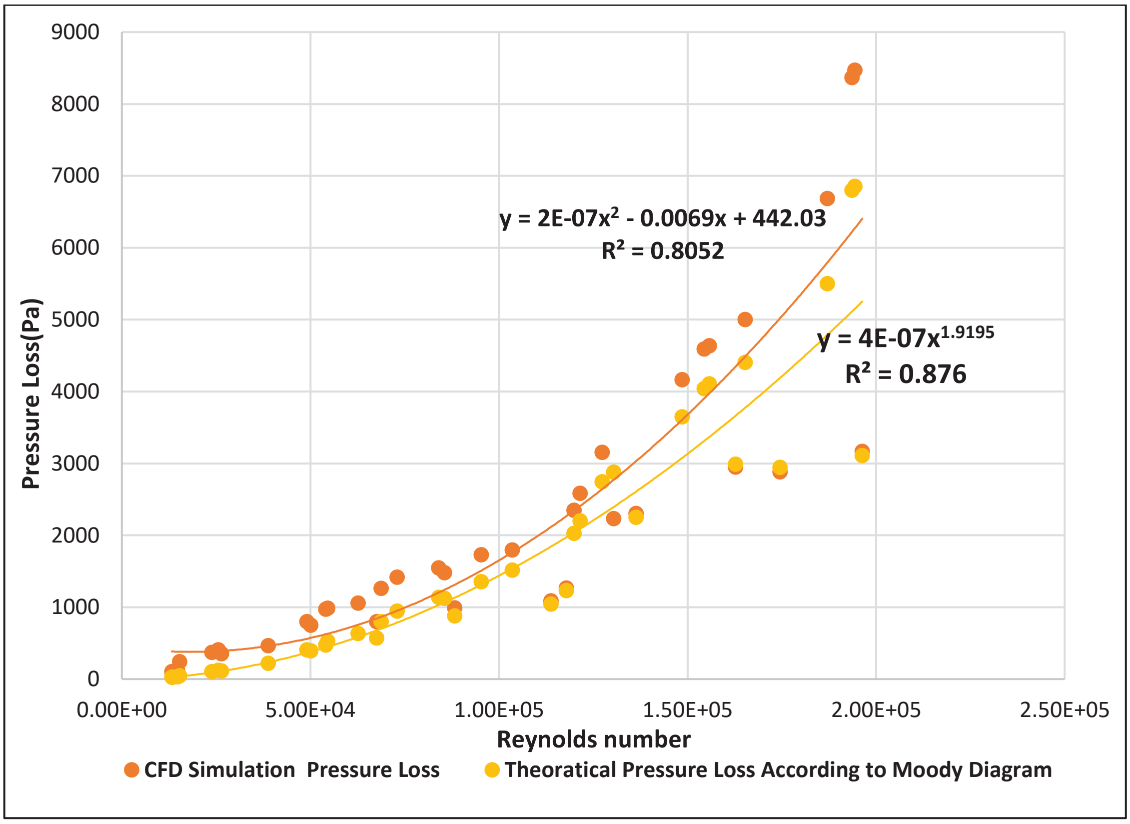

Figure 13- Theoretical and CFD simulation pressure losses comparison

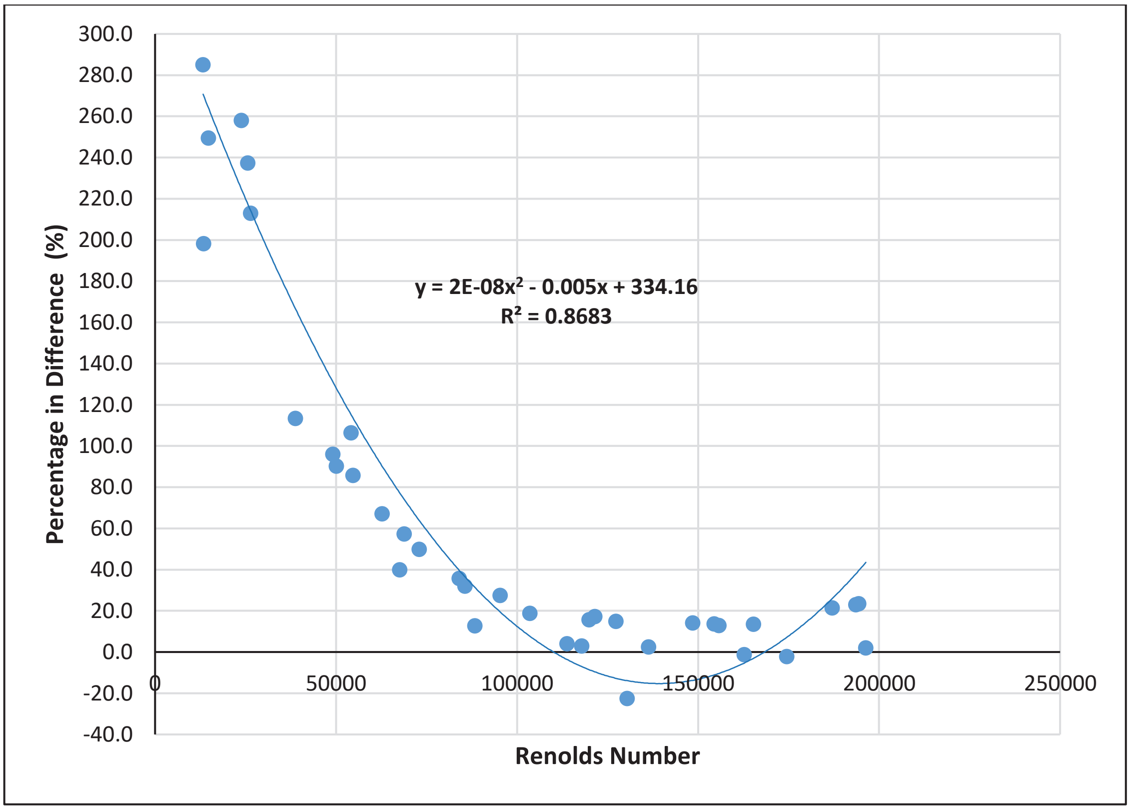

Figure 14- Theoretical and CFD simulation pressure losses percentage difference

The simulated pressure differences are compared with theoretical predictions in Figure 13. The coefficient of determination R^2 suggests that approximately 80.52% of the variability in the data was accounted by the model, indicating a moderate-to-good fit. It demonstrates that both agrees in some cases but in most cases, CFD results are much higher than the theoretical results

Considering the data distribution on Figure 14, it demonstrates that the percentage of difference between the theoretical values and CFD simulated results decrease rapidly when the Reynolds number increases. In close examination of the results, it clearly depicts a high percentage discrepancy in the transition region and the start of the turbulent region. CFD consistently predicted below 20% pressure losses in turbulent flow than theoretical models, particularly in the transitional regime more than 200% difference was observed, highlighting limitations of conventional methods. This scenario may be due to the inherent ineffectiveness of theoretical calculation method on the transition region and the start of the turbulent region.

Considering Figure 15 it clearly depicts an exponential increase of pressure loss with the inlet velocity but considering the surface roughness there was no correlation as shown in Figure 16.

In this study, validation is conducted by comparing CFD predictions against the Colebrook-White theoretical model. It is important to note that the Colebrook-White equation is an empirical correlation originally derived from the classical experimental work of Nikuradse [19] on artificially roughened pipes and subsequent commercial pipe data. While recent high-fidelity experiments, such as the Princeton Superpipe [20], provide more granular data for smooth pipes at high Reynolds numbers, the Colebrook-White relation remains the standard engineering benchmark for industrial piping design. Therefore, any deviation from the Colebrook-White curve in this study is interpreted as a deviation from the established experimental consensus represented by that equation.

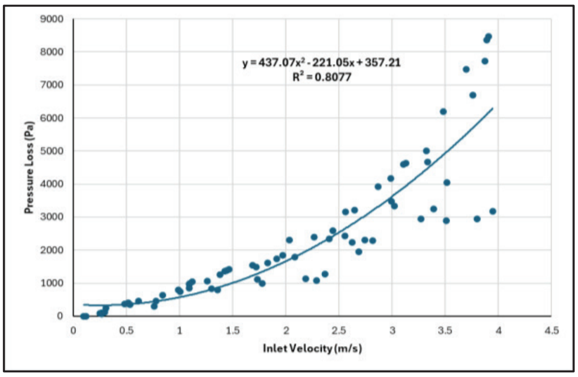

Figure 15- Correlation of inlet velocity and pressure loss with polynomial trending line

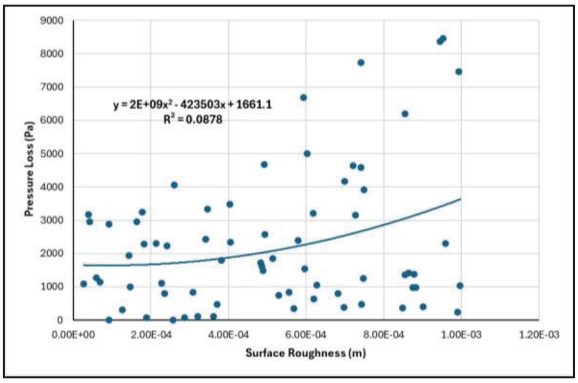

Figure 16- Correlation of surface roughness and pressure loss polynomial trending line

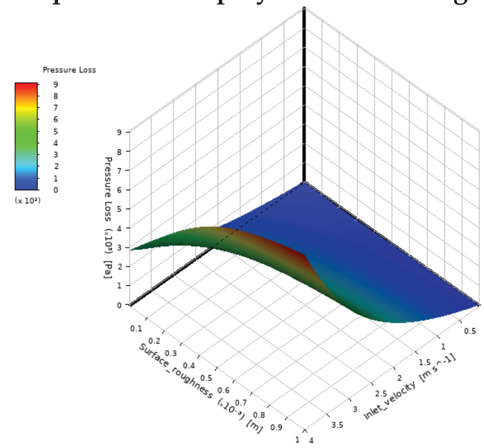

(a)

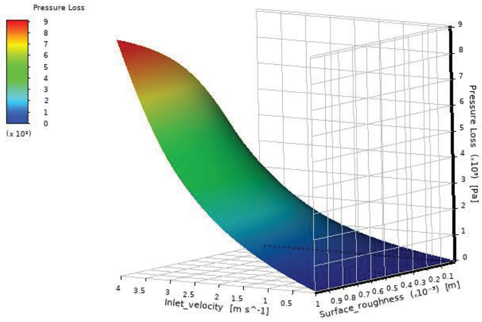

(b)

Figure 17- 3D plot of Pressure loss vs velocity vs surface roughness in X, Y, Z axis. (a) orthogonal orientation (b) orthogonal orientation with rotate in X axis

7. Conclusion

Based on the results of the CFD study conducted to analyse the variation of pressure loss in pipes, it can be concluded that the pressure loss predicted by the CFD simulations is higher compared to theoretical values. Furthermore, the study indicates that velocity has a more significant impact on pressure loss than surface roughness. This suggests that in practical applications, careful consideration should be given to the velocity profile within the pipe to accurately predict pressure loss. Additionally, while surface roughness does affect pressure loss, its influence is relatively less significant compared to velocity. Therefore, in designing efficient piping systems, controlling velocity becomes paramount for minimizing pressure loss. Considering the validity of the results, 30 to 300 y^+ results were accepted. Considering further work, experimental analysis needs to be conducted on considered flow range and to analyse that, instrumentation and test facilities need to be developed to create and analyse the turbulence and transition condition without changing flow fields.

This CFD research was conducted to analyse flow within the Reynolds number range of 2000 to 200,000 in pipes. Surface roughness was within the range of 0.001m to 2 x 10^{-6} m considering practical materials used for engineering applications. Theoretical pressure losses within the pipes were calculated using the Darcy friction factor and compared the results with CFD values. For accurate modelling of the flow, the K-epsilon turbulence model with standard wall function was used to model the turbulence flow conditions within the pipes. ANSYS Fluent 2023 R2 software tools were used to conduct the CFD experiments.

The CFD model consistently anticipated larger pressure losses as compared to the theoretical Colebrook-White baseline, which represents recognized experimental benchmarks such as Nikuradse's data [19]. This deviation is attributed to two deliberate modelling choices reflective of industrial constraints. First, the computational domain utilized a length to diameter ratio (*L/D*) of 20, resulting in developing flow conditions where wall shear stress is physically higher than in the fully developed flow assumed by theoretical correlations. Second, the application of the standard k- ϵ model in the transition region (Re < 4,000) artificially enforced turbulent viscosity, leading to conservative over predictions of friction factors.

Consequently, while the k- ϵ model lacks the sensitivity to capture the laminar to turbulent dip found in specific transition experiments, it provides a robust, conservative upper-bound estimate for pressure drop. These findings are particularly relevant for industrial engineers designing compact piping networks with short run lengths, where entrance effects and model conservatism must be accounted for to ensure sufficient pump capacity.

References

1. Reynolds, O. "An Experimental Investigation of the Circumstances Which Determine Whether the Motion of Water Shall Be Direct or Sinuous, and of The Law Of Resistance In Parallel Channels," *Proceedings of the Royal Society of London*, Vol. 35, No. 224–226, pp. 84–99, Dec. 1883, doi: https://doi.org/10.1098/rspl.1883.0018

2. Avila, M., Barkley, D. and Hof, B. "Transition to Turbulence in Pipe Flow," *Annual Review of Fluid Mechanics*, Vol. 55, No. 1, pp. 575–602, Jan. 2023, doi: https://doi.org/10.1146/annurev-fluid-120720-025957

3. Kieckhefen, P., Pietsch, S., Dosta, M. and Heinrich, S. "Possibilities and Limits of Computational Fluid Dynamics–Discrete Element Method Simulations in Process Engineering: A Review of Recent Advancements and Future Trends," *Annual Review of Chemical and Biomolecular Engineering,* Vol. 11, No. 1, pp. 397–422, Jun. 2020, doi: https://doi.org/10.1146/annurev-chembioeng-110519-075414

4. Zawawi, M. H., et al. "A Review: Fundamentals of Computational Fluid Dynamics (CFD)," *Green Design and Manufacture: Advanced and Emerging Applications* Vol. 2030, No. 1, 2018, doi: https://doi.org/10.1063/1.5066893

5. Ahsan, M. "Numerical Analysis of Friction Factor for a Fully Developed Turbulent Flow Using k–ε Turbulence Model with Enhanced Wall Treatment," *Beni-Suef University Journal of Basic and Applied Sciences*, Vol. 3, No. 4, pp. 269–277, Dec. 2014, doi: https://doi.org/10.1016/j.bjbas.2014.12.001

6. Kadivar, M., Tormey, D. and McGranaghan, G. "A Review on Turbulent Flow Over Rough Surfaces: Fundamentals and Theories," *International Journal of Thermofluids,* Vol. 10, p. 100077, May 2021, doi: https://doi.org/10.1016/j.ijft.2021.100077

7. Launder, B. E. and Spalding, D. B. "The Numerical Computation of Turbulent Flows," *Computer Methods in Applied Mechanics and Engineering*, Vol. 3, No. 2, pp. 269–289, Mar. 1974, doi: https://doi.org/10.1016/0045-7825(74)90029-2

8. "Ansys Student Versions | Free Student Software Downloads," www.ansys.com. https://www.ansys.com/academic/students

9. Salama, A. "Velocity Profile Representation for Fully Developed Turbulent Flows in Pipes: A Modified Power Law," *Fluids*, Vol. 6, No. 10, p. 369, Oct. 2021, doi: https://doi.org/10.3390/fluids6100369

10. Kadivar, M., Tormey, D. and McGranaghan, G. "A Review on Turbulent Flow Over Rough Surfaces: *Fundamentals and theories," International Journal of Thermofluids,* Vol. 10, p. 100077, May 2021, doi: https://doi.org/10.1016/j.ijft.2021.100077

11. Carney, S. P., Engquist, B. and Moser, R. D. "Near-Wall Patch Representation of Wall-Bounded Turbulence," *Journal of Fluid Mechanics,* Vol. 903, Sep. 2020, doi: https://doi.org/10.1017/jfm.2020.658

12. El, G. K., Schlatter, P., Noorani, A., Fischer, P., Brethouwer, G. and Johansson, A. "Direct Numerical Simulation of Turbulent Pipe Flow at Moderately High Reynolds Numbers," *Flow, turbulence and combustion,* Vol. 91, No. 3, pp. 475–495, Jul. 2013, doi: https://doi.org/10.1007/s10494-013-9482-8

13. Gopalan, H., Heinz, S. and Stöllinger, M. "A Unified RANS–LES Model: Computational Development, Accuracy and Cost," *Journal of Computational Physics* Vol. 249, pp. 249–274, Sep. 2013, doi: https://doi.org/10.1016/j.jcp.2013.03.066

14. Hall, S. "Fluid Flow," *Branan's Rules of Thumb for Chemical Engineers,* pp. 1–26, 2012, doi: https://doi.org/10.1016/b978-0-12-387785-7.00001-3

15. Joseph, D. D. and Yang, B. H. "Friction Factor Correlations for Laminar, Transition and Turbulent Flow in Smooth Pipes," Physica D," *Nonlinear Phenomena*, Vol. 239, No. 14, pp. 1318–1328, Jul. 2010, doi: https://doi.org/10.1016/j.physd.2009.09.026

16. Kadivar, M., Tormey, D. and McGranaghan, G. "A Review on Turbulent Flow Over rough surfaces: Fundamentals and Theories," *International Journal of Thermofluids*, Vol. 10, p. 100077, May 2021, doi: https://doi.org/10.1016/j.ijft.2021.100077

17. The Efficient Engineer, "Understanding Laminar and Turbulent Flow," *YouTube*. Sep. 08, 2020. Available:https://www.youtube.com/watch?v=9A-uUG0WR0w

18. Idealsimulations, "Turbulence Models in CFD - RANS, DES, LES and DNS," *IdealSimulations*, Aug. 30, 2019. https://www.idealsimulations.com/resources/turbulence-models-in-cfd/

19. Nikuradse, J., 1933. Strömungsgesetze in Rauhen Rohren. VDI-Forschungsheft 361, Berlin. English translation: Laws of Flow in Rough Pipes, *NACA Technical Memorandum 1292*. Available at: https://digital.library.unt.edu/ark:/67531/metadc63009/

20. McKeon, B. J., Swanson, C. J., Zagarola, M. V., Donnelly, R. J. and Smits, A. J. "Friction Factors for Smooth Pipe Flow," *Journal of Fluid Mechanics,* Vol. 511, pp. 41–44, Jul. 2004, doi: https://doi.org/10.1017/s0022112004009796